THE JOURNAL OF PHYSICAL CHEMISTRY C

Article

Cite This: J. Phys. Chem. C 2019, 123, 16804−16812

pubs.acs.org/JPCC

Reactive Force Field for Simulations of the Pyrolysis of Polysiloxanes into Silicon Oxycarbide Ceramics

Ilia Ponomarev,[†] Adri C. T. van Duin,[‡] and Peter Kroll*[,†]

[†]Department of Chemistry and Biochemistry, The University of Texas at Arlington, 700 Planetarium Place, Arlington, Texas 76019, United States

[‡]Department of Mechanical and Nuclear Engineering, Pennsylvania State University, University Park, Pennsylvania 16802, United States

ABSTRACT: We provide a new reactive force field (ReaxFF) for simulations of silicon oxycarbide (SiCO) ceramics and of their syntheses from inorganic polymer precursors. The validity of the force field is extensively tested against experimental and computational thermochemical data. Its performance in simulation at elevated temperatures is gauged by the results of comprehensive ab initio molecular dynamics simulations. We apply the force field to the formation of amorphous SiCO in a simulated polymer pyrolysis. Modeling results are in good agreement with experimental observations and allow new insights into the formation of graphene segregations embedded in an amorphous oxycarbide matrix. The new ReaxFF for Si−C−O−H compounds enables large-scale and long-time atomistic simulations with unprecedented fidelity.

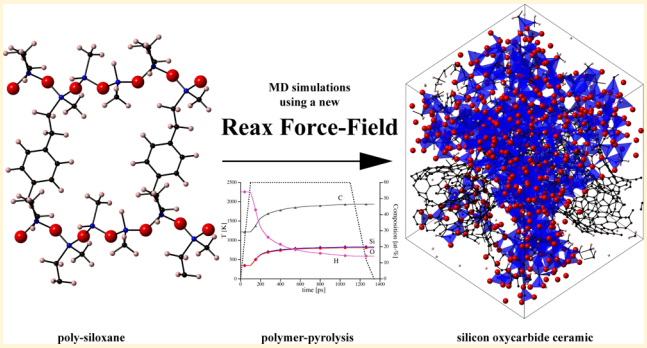

1. INTRODUCTION

Silicon oxycarbide (SiCO) materials possess a wide range of attractive properties such as chemical durability,[1] high-temperature stability,[2] high creep resistance, and other specific mechanical properties.[3,4] SiCO materials are used or proposed to be used in applications for gas separation,[5,6] thermal protection,[7] radiation protection,[8,9] advanced drug delivery,[10] low-κ dielectric electronics,[11] and energy storage.[12] Synthesis of SiCO proceeds via "bottom-up" processes: sol−gel syntheses,[13] polymer-to-ceramic routes,[14] and different flavors of vapor deposition methods.[15−17]

Composition and structure of SiCO materials depend on the involved chemistry, details of the processing, and, not at least, the thermal history of the material. Synthesized at temperatures below 1200 °C, the material remains amorphous, and crystallization occurs only at significantly higher temperatures.[18] Even in the amorphous state, significant differences exist. For instance, low-κ SiCO thin films for electronic applications contain significant amounts of hydrogen and methyl groups.[19] Here, we focus on carbon-rich SiCO ceramic materials produced by the polymer-to-ceramic route. These ceramics exhibit a "SiCO glass" phase with the so-called "free" carbon embedded in the matrix[14]

$$SiC_{x+y}O_{2(1-x)} = \{x\cdot SiC + (1-x)SiO_2\} + y\cdot C_{free}$$

The SiCO glass, a stoichiometric mixture of SiO_2 and SiC, comprises a random network of Si−O and Si−C bonds forming mixed SiC_nO_{4-n} tetrahedra.[18,20,21] Carbon within the glass appears ("carbidic") in CSi_4 tetrahedra similar to that in SiC, while O atoms bridge between Si atoms as in silica glass. The "free" carbon phase appears similar to graphite or graphene.[22] Stoichiometric SiCO glass without "free" carbon can be synthesized.[3] The morphology of the "free" carbon, its interface to the glass matrix, as well as the amount of hydrogen remaining in the material are hotly debated issues in concurrent research.[23,24]

Atomistic modeling and accurate density functional theory (DFT) calculations have contributed to better understanding local structures in SiCO materials. The SiCO glass has been characterized early on,[25] and various interfaces between SiCO and "free" carbon have been studied.[26] Combining computational and experimental ^{29}Si NMR illuminated bonding at interfaces in amorphous SiCO.[21] Unfortunately, DFT calculations are computationally very expensive, which limits model sizes to a few hundred atoms and simulation times to below 1 ns. Through empirical potential simulations, on the other side, it is feasible to explore the mechanical properties of SiCO in models with millions of atoms extending several nanometers.[27] However, these models lack accuracy of chemical bonding, proper atomic environments, and acceptable thermochemistry.

The reactive force field (ReaxFF)[28] bridges the gap between accurate DFT simulations and empirical potential simulations. It achieves a level of accuracy approaching DFT simulations for a wide set of molecular reactions in the gas phase[28] and on

Received: April 24, 2019
Revised: June 6, 2019
Published: June 10, 2019

DOI: 10.1021/acs.jpcc.9b03810
J. Phys. Chem. C 2019, 123, 16804−16812

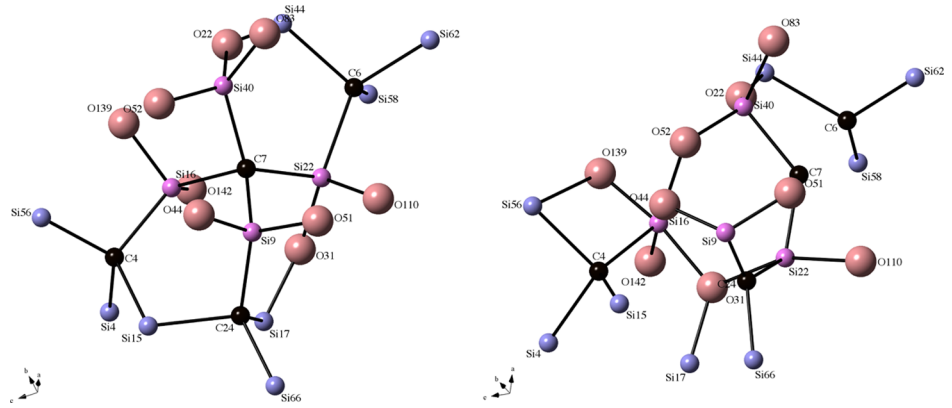

Figure 1. Fragment of the model of stoichiometric SiCO glass (composition $Si_{104}C_{24}O_{160}$) before (left) and after (right) 100 ps long MD simulation at 300 K using Newsome ReaxFF parameters. We emphasize four mixed SiC_nO_{4-n} tetrahedral (Si in magenta) bonding to C (label C7). Sphere represent atoms: C (black), Si (blue and magenta), O (red).

surfaces.[29,30] At the same time, ReaxFF is several orders of magnitude less computationally expensive, which allows modeling chemical processes in larger systems for longer simulation times as compared to DFT simulations. A few studies of modeling reactive processes in SiCO using ReaxFF have been published recently.[31−33] As we will show further below, the Newsome et al.[31] ReaxFF parameterization used in these studies as well as Soria et al.[29] parameterization developed later fails to model many distinct features of SiCO, and resulting structures are inadequate. Thus, to achieve the desired level of fidelity for a wide range of local atomic configurations, it requires careful development of the numerous parameters describing interaction.

Here, we represent new ReaxFF parameters describing interactions among Si, C, O, and H atoms in SiCOH materials. Starting with an existing ReaxFF parameterization,[31] we take advantage of data of several thousands of DFT-computed models of SiCO and involve a self-learning process to eliminate pitfalls and traps. The new ReaxFF is then applied to simulate the polymer-to-ceramic conversion of a cross-linked polysiloxane precursor.

2. COMPUTATIONAL METHODS

The ReaxFF has been designed to model chemical reaction through molecular dynamics (MD) simulations.[28] Guided by quantum chemical calculation, the energy of a system is partitioned into a variety of terms, including two-center covalent bond energy, Coulomb interactions, van der Waals interactions, a description for under- and overcoordination of atoms, angular and torsional terms, and additional bond conjugation and penalties. A detailed description is given in ref 28. A typical parameter set comprises 39 general parameters, another 32 parameters per atom, and 16 parameters per bond, plus 7 additional off-diagonal bond parameters for heteroatomic bonds, 7 angular parameters, 5 torsion parameters, and 4 parameters to describe hydrogen bonding. With more than 100 parameters to describe a system such as polysiloxane and SiCO ceramics, the chance of overparameterization is immanent. Therefore, deriving a high-fidelity parameter set requires careful optimization against quality data, either experimental or computed via quantum mechanics methods.

We started with an existing parameter set for SiCO developed by Newsome et al.[31] This force field was developed with the purpose to model the oxidation of silicon carbide. It incorporates essential thermochemistry of the Si−C−O system, including enthalpies of formation of SiC and SiO_2, reaction enthalpies of carbothermal reduction of SiO_2, and enthalpies of formation for a variety of small molecules. We then added recent force field parameters by Srinivasan[34] for the description of carbon−carbon interactions. Thereafter, we provided structure and energy data from our library of DFT-optimized SiCO models. The library comprises over 10 000 hypothetical crystalline SiCO structures[35] and more than 1000 models of amorphous SiCO generated via a network algorithm or through melt-quench ab initio MD (aiMD) simulations.[21,25,26,36,37] Using the accumulated data, we optimized force field parameters for SiCOH with the ReaxFF software.[28] At this stage, we achieved mapping of DFT energy differences to ReaxFF energy differences. However, the reverse mapping lacked strong correlation. Consequently, we augmented the training set with $SiC_xO_yH_z$ models created by ReaxFF itself via melt-quench simulations and subsequently optimized in DFT. This recursive learning strategy expanded the range of configurations explored and enabled the development of robust force field parameters.

The DFT[38] calculations in this work are carried out with the Vienna ab initio simulation package.[39,40] We use the projector augmented wave[41,42] method and approximate electron exchange and correlation by the Perdew−Burke−Ernzerhof generalized gradient approximation.[43,44] The DFT-D2 method of Grimme[45] is applied to account for van der Waals interactions. The energy cutoff for the expansion of the wave function into the plane-wave basis is 500 eV. aiMD simulations are performed at reduced energy cutoff under constant volume with a time step of 1 fs.

MD simulations with ReaxFF are performed with the large-scale atomic/molecular massively parallel simulator software[46] distributed by Sandia National Laboratories and its Reax/c user's package.[47] We apply the Bussi−Donadio−Parrinello thermostat (temp/csvr command)[48] for temperature control. Depending on the hydrogen content of the model, we use a time step of 0.1−1.0 fs for the integration of the equations of motion.

3. RESULTS AND DISCUSSION

3.1. Identifying the Need for a New Force Field. A proper Si−C−O−H force field must provide accurate description of the stoichiometric SiCO glass phase that not

DOI: 10.1021/acs.jpcc.9b03810
J. Phys. Chem. C 2019, 123, 16804−16812

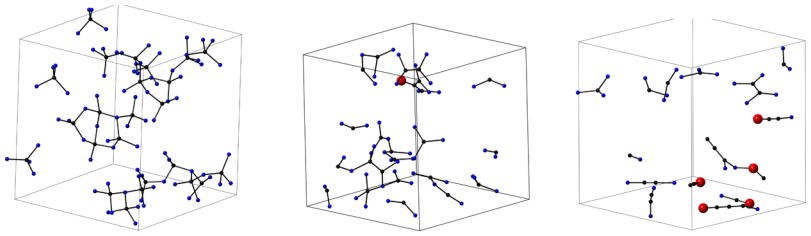

Figure 2. Model of stoichiometric SiCO glass (composition $Si_{104}C_{24}O_{160}$) before (left) and after 100 ps long MD simulation at 1200 K (center) and 2000 K (right) using Newsome ReaxFF parameters. Only C atoms and their nearest neighbors are displayed.

only develops during the synthesis of SiCO ceramics[3,13,14,18] but also occurs at reaction fronts during the oxidation of SiC.[49,50] A fundamental characteristic of the SiCO glass is SiC_nO_{4-n} tetrahedra.[18,20] These so-called mixed tetrahedra not only emerge in the glass phase of the sol−gel processed or polymer-derived SiCO ceramics[51] but also develop upon oxidation of SiC (starting with only SiC_4 tetrahedra). Unfortunately, the parameter sets developed by Newsome et al. and Soria et al. cannot properly describe mixed SiC_nO_{4-n} tetrahedra, as shown in Figure 1. While both parameterizations share the same issues, we focus our comparison on the parameter set of Newsome et al. because we used this as the starting point for our work. A perfect network of SiCO glass previously optimized using DFT is severely distorted in a MD simulation at 300 K using Newsome et al. parameters. The force field ruptures several Si−C bonds in mixed SiC_nO_{4-n} tetrahedral units, creating defects such as under- and overcoordinated sites.

We find another deficiency of the existing parameters by comparing ReaxFF energies with those calculated by DFT for stoichiometric SiCO glass models. This is shown in detail further below, where we highlight the performance of the new set of parameters developed. Finally, the parameter set of Newsome et al. does not catch properly the remarkable kinetic stability of stoichiometric SiCO glass. Network models of glass SiCO are kinetically stable in aiMD simulations at elevated temperatures, for example, at 2600 K for 20 ps and longer.[25] The aiMD simulations show "melting" (i.e., breaking of bonds) only at higher temperatures. In sharp contrast, a ReaxFF MD simulation using the parameter set of Newsome et al. significantly deteriorates the model already at 1200 K, a temperature at which a-SiCO remains stable in the experiment. Simulation at 2000 K ruptures the model completely and leaves none of the existing carbidic carbon units, CSi_4-tetrahedra, intact (see Figure 2). The formation of C−C and C−O bonds in the simulation goes along with under-coordination of Si and formation of Si−Si bonds in the final model.

Deficiencies of the Newsome parameters have recently been identified by Takamoto et al.[52] Their study underlines the call for developing a new set of parameters for ReaxFF, which can properly handle the variety of Si−C−O interactions occurring in polysiloxanes and SiCO ceramics.

3.2. Performance of the Newly Developed Force Field. The significant improvement of correspondence between DFT-computed energies and ReaxFF energies using the new parameter set is shown in Figure 3. We compare DFT-computed energies for a standard set[25] of network models with composition $Si_{48}C_{16}O_{64}$ with energies computed by ReaxFF. In comparison with the previous force field, the newly developed force field parameters UTA1 yield almost a unit slope,

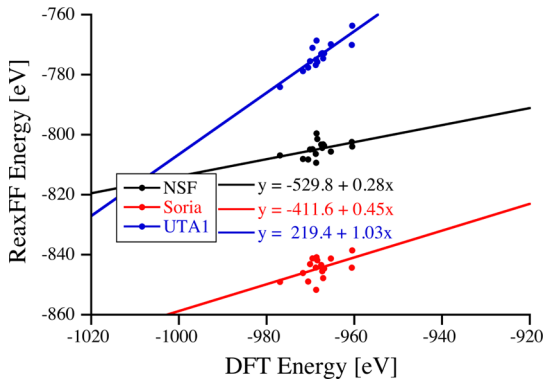

Figure 3. Comparison of DFT energies of stoichiometric SiCO glass models with composition $Si_{48}C_{16}O_{64}$ with ReaxFF energies using parameters of Newsome et al.,[31] Soria et al.,[29] and UTA1 ReaxFF parameters.

indicating that energy differences in DFT agree with those in ReaxFF. While the graph displays the relation for models with composition $Si_{48}C_{16}O_{64}$ only, we obtain equivalent agreement for all other stoichiometric compositions.

Besides achieving correspondence of energy differences, we also improve the dynamic stability of SiCO glass structures. We performed MD simulations of stoichiometric SiCO with composition $Si_{104}C_{24}O_{160}$ (24·SiC + 80·SiO_2, 24 mol % SiC) using two different sets of models, each comprising three independent structures. One cohort exhibits a random distribution of mixed SiC_nO_{4-n} tetrahedra. This is typical for SiCO glass synthesized at about 1000 °C.[2,18,53] Models in the second set are "segregated", with the preference of SiC_4 and SiO_4 tetrahedra on the cost of mixed units. One structure even exhibits a large SiC nucleus embedded by SiO_2. Such configurations are typical for the partitioned yet still disordered state of SiCO materials annealed to higher temperatures (1200 °C).[18] They also occur at the interface between silicon carbide and its natural oxide, silica. After heating to 2000 K and annealing at this temperature for 100 ps, we analyzed all structures. We focus on persistence and stability of (carbidic) C atoms within CSi_4 tetrahedra and of mixed SiC_nO_{4-n} tetrahedra. Figure 4 displays one of the "random" a-SiCO models before and after completed simulation. Structural information on the models is summarized in Tables 1 and 2.

Overall, the new force field provides stability of carbidic carbon at elevated temperatures and retains most of the mixed SiC_nO_{4-n}-tetrahedral environments. This will be important for modeling phase separation in SiCO, which involves the formation of SiC nuclei. Moreover, it is essential for the simulation of pyrolysis of polymer precursors, for example, poly-methyl-siloxanes. These encounter a Kumada-like rearrangement[54] as their most critical step.[14] Thermal activation

DOI: 10.1021/acs.jpcc.9b03810
J. Phys. Chem. C 2019, 123, 16804−16812

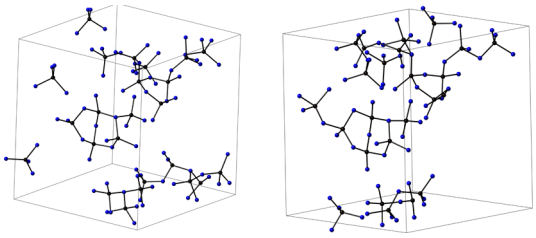

Figure 4. Model of stoichiometric SiCO glass (composition $Si_{104}C_{24}O_{160}$) before (left) and after (right) 100 ps long MD simulation at 2000 K using the UTA1 ReaxFF parameter set. Only C atoms and their nearest neighbors are displayed.

Table 1. Amount (in %) of Carbidic C Atoms in $Si_{104}C_{24}O_{160}$ Retaining Tetrahedral Coordination (CSi_4) after 100 ps Simulation at 2000 K

models	NSF	Soria	UTA1
random	3	22	83
segregated	4	17	96
all models	3	26	90

leads to the cleavage of Si−O bonds and insertion of carbon forming Si−C bonds in the polymer backbone. This process yields the random distribution of mixed SiC_nO_{4-n} tetrahedra, even if the molecular or polymeric precursors have a singular distinct environment only.[18,55]

Besides providing description of the SiCO glass, our ReaxFF parameterization is also suitable to model pure SiO_2 glass. We performed melt-quench simulations to generate amorphous SiO_2 models. Starting with a 1032 atom model at 4000 K, we quenched the system with a rate of 5 K/ps. Throughout the simulation, we maintained a *NPT* ensemble, allowing the density of a-SiO_2 to adjust. A brief analysis of structural parameters of the a-SiO_2 model is given in Table 3 and compared with data from models generated similarly using the parameters of Newsome et al.[31] We also include results obtained using yet another set of ReaxFF parameters especially designed for modeling a-SiO_2.[56,57] Our new ReaxFF parameters yield less than 5% of defects such as under- or overcoordinated Si and O atoms. Density, average Si−O bond length, and average Si−O−Si bond angle are close to the experimental values.[58] Overall, our model compares well to structures obtained using a parameterization of ReaxFF developed especially for silicates.[56,57]

The "free" carbon phase is characteristic of most SiCO ceramics. Its genesis during synthesis and processing is the focus of many investigations, and tailoring its emergence through the molecular or polymeric structure is a key issue for synthesis. Indeed, the development of the interface between the glass matrix and "free" carbon is still an unresolved topic. A library of SiCO models comprising "free" carbon has been part of the parameter development.[21,26] Here, we show the performance of the new ReaxFF parameter set for the generation of SiCO structures via melt-quench MD simulations. Twenty models of composition $Si_5CO_8 + 10C_{free}$, each comprising 120 atoms and a density of 2.2 g/cm^3, were generated via melt-quench simulations using a cooling rate of 20 K/ps. The models were finally optimized within ReaxFF. Subsequently, we switched to DFT calculations for direct comparison between ReaxFF energies and DFT energies. We computed the energy of each model at the beginning and the end of its DFT optimization. The difference between the two energies is a measure of "proximity" of potential energy surfaces of ReaxFF and DFT. Figure 5 provides a comparison for different compositions, with and without free carbon, generated within ReaxFF and further optimized in DFT.

Structures generated with the new parameter set come out much closer to the DFT-optimized state than the models generated with parameters of Newsome et al. The average energy gained during DFT optimization (0.22 eV/atom compared to 0.69) is much lower for the new than for the previous parameter set. Although we do not obtain perfect agreement, the new ReaxFF parameter set generates models very similar to those obtained via DFT melt-quench simulations. Figure 6 shows a comparison between models generated via ab initio and ReaxFF melt-quench MD simulations for the composition $Si_5CO_8 + 10C_{free}$ with an initial density of 2.2 g/cm^3. Both models comprise a layer of "SiCO glass" sandwiched between a buckled graphene layer of "free carbon" phase. Note that size, periodic boundary conditions, and composition have a major impact on the final structure.

SiCO ceramics are produced by the pyrolysis of molecular or polymeric precursors that contain substantial amounts of hydrogen.[13,14] Presence and content of hydrogen play a significant role in carbon segregation,[32] electric properties of the final material,[15] or withstanding radiation damage by a-SiCO(:H).[8] We included parameters for the interaction between H and the other elements, C, O, and Si, from Newsome et al.[31] Some modifications were necessary to avoid unphysical bonding situations, and once again we located optimum parameters through repeating learning cycles of model generation and DFT optimization. Results for SiCOH models are quite similar to what has been shown before (e.g., Figure 5). Here, we support "robustness" and "proximity" of ReaxFF and DFT energy minima in yet another way. We first generated a model of composition $Si_{25}C_{55}O_{40}H_{12}$ via melt-quench MD simulation (cooling rate 25 K/ps) in ReaxFF. Thereafter, we started a cycle of optimization first using

Table 2. Amount (in %) of Unchanged SiC_nO_{4-n} Tetrahedral in $Si_{104}C_{24}O_{160}$ after 100 ps Simulation at 2000 K[a]

	NSF		Soria		UTA1	
Si unit	random	segregated	random	segregated	random	segregated
SiO_4	0	1	25	40	76	70
SiO_3C	0	0	6	10	76	67
SiO_2C_2	0	0	0	0	62	82
$SiOC_3$	0	0	0	3	82	86
SiC_4		0		0		95
all units	0		18		74	

[a]ReaxFF parameters used refer to Newsome et al.[31] (NSF), Soria et al.[29] (Soria), and those developed in this work (UTA1)

DOI: 10.1021/acs.jpcc.9b03810
J. Phys. Chem. C 2019, 123, 16804−16812

Table 3. Structural Parameters of SiO_2 Models (1032 Atoms) Generated via Melt Quench Using ReaxFF with Original Newsome Parameters[31] (NSF), Pitman Parameters,[56,57] and the Parameters Presented in This Work (IP)[a]

		number of atoms per model adopting coordination				number of bonds per model		average	
force field	ρ [g/cm^3]	Si[3]	Si[5]	O[1]	O[3]	Si–Si	O–O	d_{Si-O} [Å]	⟨Si–O–Si⟩ [deg]
NSF	2.52	1	22	15	37	0	4	1.60	148
UTA1	2.17	13	9	13	9	1	2	1.62	146
Pitman	2.10	9	10	6	7	0	2	1.64	138
Exp.	2.20							1.61	142–147

[a]Experimental data (Exp.) are taken from ref 58.

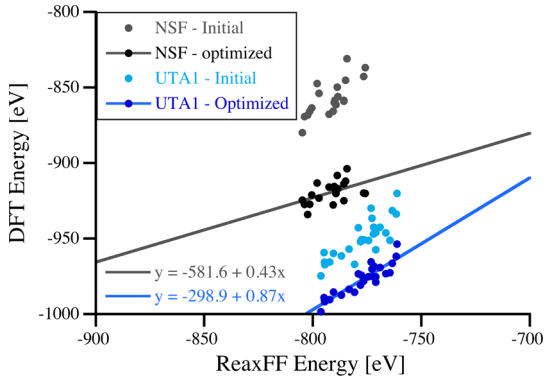

Figure 5. Energies of the models Si_5CO_8 + $10C_{free}$ (ρ = 2.2 g/cm^3) generated via ReaxFF melt-quench simulation and optimized in DFT. "Initial"—first energy computed via DFT. "Optimized"—final DFT energy. NSF—original Newsome force field.[31] UTA1—force field parameters developed in this work.

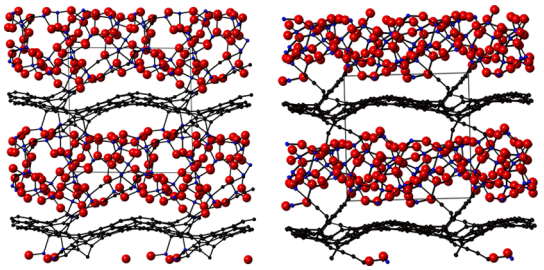

Figure 6. Amorphous models [left: DFT; right: ReaxFF using UTA1 parameters] of Si_5CO_8 + $10C_{free}$ (192 atoms) generated via melt-quench MD simulation with a cooling rate of 12.5 K/ps starting from 5000 K.

ReaxFF and then DFT. After the first DFT optimization, we keep the volume of the model constant. The cycle was then repeated several times. If potential energy surfaces of ReaxFF and DFT would not correspond well to each other, this cycling would produce more and more different structures. This happens, indeed, if "cycling" is performed using a Tersoff potential with parameters taken from refs[59−62] and DFT. Using ReaxFF parameters of Newsome et al. and performing "cycling" create many diverging structures as well. With the new parameter set, on the other side, models converge back to almost identical positions in every cycle. The sequence of energies of optimized structures is shown in Figure 7. We followed the same process with a second model generated first using ab initio melt-quench simulations in DFT and performed repeated optimizations in DFT, followed by optimizations using ReaxFF. Here too, models converge back to almost the initial positions after every cycle.

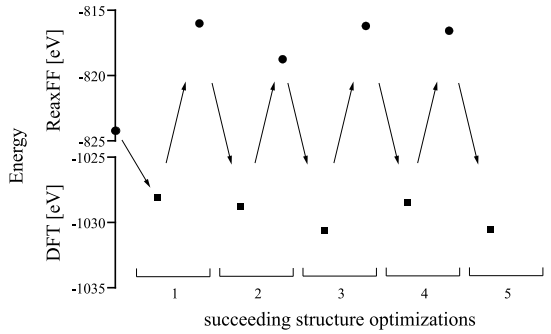

Figure 7. Final energies in repeated optimizations of the SiCOH model (composition $Si_{25}C_{55}O_{40}H_{12}$) within DFT and ReaxFF.

Before we go on and apply the new force field to model chemical processes, we can summarize the accomplishments of the parameter development. The new force field has been adjusted to provide a mapping of DFT energy differences to ReaxFF energy differences. For a variety of SiCO models, including those with "free" carbon, we show that energy differences agree on average. Moreover, modeling structures within ReaxFF and subsequently optimizing them in DFT show that the reverse mapping holds as well. Thus, ReaxFF simulations of SiCO do not provide artificial structures that are local minima only with respect to the ReaxFF. These situations have been eliminated by the extensive learning strategy by repeatedly using the results of ReaxFF simulations as test models for the development process.

Despite the obvious progress, our current set of ReaxFF parameters for SiCO is not perfect. For instance, we notice higher tolerance of ReaxFF for three-coordinated Si[3] and O[3] species. These rarely appear in DFT-generated models of SiCO, and reactivity of Si[3] is well-known in experiments.[63] We also notice that modeling SiCO by ReaxFF yields a discernible preference for the density of SiCO depending on the composition. Simulations at constant volume show clear dependence of energy on density. On the other side, this dependency is much weaker when using network modeling or aiMD simulations at constant volume to model SiCO.[25] Such remaining imperfections will be addressed in future work. With the new ReaxFF parameters at hand, we can advance to the simulations of SiCO formation via thermal treatment of polymer precursors.

3.3. Modeling the Polymer-to-Ceramic Conversion: Pyrolysis and Annealing of PHMS/DVB. Providing deeper insight into processing of polymers into ceramics is essential for tailoring materials properties and for developing optimized chemical precursors. Quantum chemical calculations provide accurate simulations, but unfortunately hit barriers are associated with size and time. Simple (semi-) empirical

DOI: 10.1021/acs.jpcc.9b03810
J. Phys. Chem. C 2019, 123, 16804−16812

potentials (e.g., Tersoff[64]) on the other side lack accuracy (and ability) in the description of chemical reactions and processes. This is where the ReaxFF finds its application: adjusted to accurate quantum chemical calculations with the benefits of scalability of empirical simulations. As an example of a polymer-to-ceramic conversion, we model the pyrolysis of polymethylhydridosiloxane (PMHS) cross-linked with divinylbenzene (DVB).[65] This polymeric precursor has been used for the synthesis of bulk and porous SiCO ceramics.[66,67] Ceramics obtained after pyrolysis are well characterized and comprise an amorphous SiCO phase with high "free" carbon content.[67] Materials synthesized from PMHS and DVB have been investigated as Li-anode materials[68,69] for environmental remediation,[24] sensors,[70] and gas separation[6] and as molecular sieves.[24]

We start our simulation with modeling a cross-linked PMHS/DVB polymer, connecting different strands of PMHS with DVB. Figure 8 (left) shows a fragment of the structure.

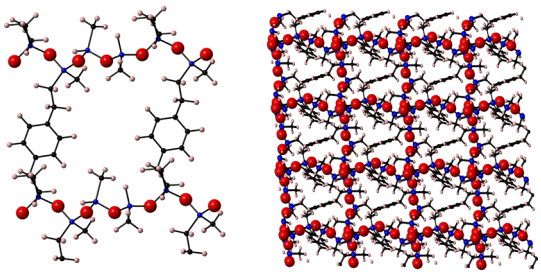

Figure 8. Left—fragment of the PHMS/DVB polymer structure. Right—entangled 3D polymer structure. Spheres are Si (blue), C (black), O (red), H (pink).

Note that the ratio of polymer units [−Si(H,Me)−O−] to double bonds [−H_2C═CH−] of the DVB vinyl group is 2:1. This corresponds to a mass ratio of 4:1 between PMHS polymer units and the molecular DVB. Essentially, it leaves every other Si−H bond available for further reactions. The fragment shown in Figure 8 is then interpenetrated by a second similar cross-linked polymer, yielding an entangled three-dimensional (3D) polysiloxane, as shown in Figure 8 (right). The model is replicated in all three directions and placed into a rectangular box with dimensions of approximately 4.0 × 4.5 × 4.0 nm^3 under periodic boundaries. The composition is $Si_{512}C_{1792}O_{512}H_{3328}$ (6144 atoms) with a density of 1.08 g/cm^3. This polymer model serves as the starting configuration for further simulations.

After an initial equilibration at room temperature, we heat the model to 2500 K at constant volume with a rate of 25 K/ps. This process is required to observe reactions within feasible simulation times.[71] Experimental processing conducts the pyrolysis with a heating rate of 5 K/min to temperatures between 900 and 1200 °C.[14,68] Once the maximum temperature is reached, we anneal the system for 1 ns (5×10^6 time steps using Δt = 0.2 fs). Throughout the annealing, we maintain a constant pressure of 2000 bar to prevent "foaming" of the model. We also monitor the formation of gaseous reaction products, H_2, CO, CO_2, H_2O, O_2, CH_2O, C_2H_2, and C_2H_4. Every 5 ps, we remove persistent gas molecules. This process effectively simulates the evolution of gaseous species as monitored by mass spectrometry.[72] Finally, we cool the system down to 0 K while continuing removal of the gaseous species as they appear. In Figure 9, we display the temperature profile for the simulation together with the evolution of composition of the system.

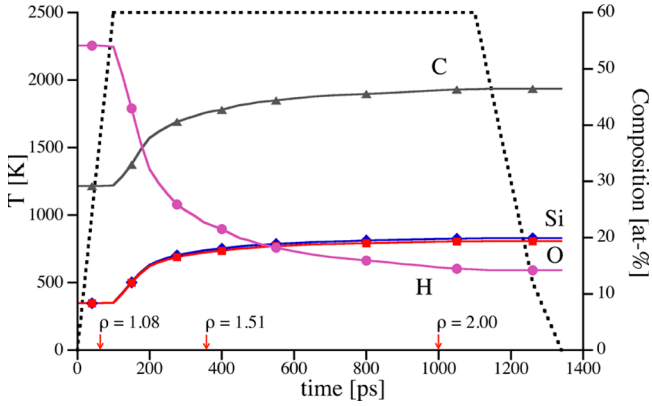

Figure 9. Time-temperature scheme (black dotted line) of simulated annealing of the PMHS/DVB polymer. The second *y*-axis refers to the composition of the model (in atom %) as a function of annealing time. Density (in g/cm^3) milestones are marked with arrows on the x-axis.

Details of the chemical process will be given elsewhere. In brief, first processes we observe are H and CH_3 groups forming gaseous CH_4, leaving behind undercoordinated Si. These quickly react in various ways, creating Si−Si bonds, forming three-coordinated O, or terminating by H. With increasing temperature, the polymer −Si−O− backbone becomes flexible enough to allow insertion of methyl groups into the polymer chain (Kumada-like rearrangement). Only very few CO molecules develop, and the Si/O ratio is almost maintained throughout the simulation. At the same time, DVB units dissociate, leaving behind vinyl fragments and phenyl rings. The latter then start to form larger agglomerates such as poly-aromatic carbon. The latter process is facilitated by the openness of the polymer backbone, which allows large windows to appear in the structure suitable for the migration of larger carbon units. Ultimately, we observe segregation of tubular carbon and SiCO glass (Figure 10). At this stage of the simulation, mass loss happens through the removal of H_2 only.

Composition and density of models obtained, averaged over two simulations, are summarized in Table 4 and compared with experimental results.[4,51,73] Mass loss and final density match experimental data auspiciously. In the course of the simulations, the linear dimensions of the model shrink by 25%. The final structure of the a-SiCO ceramic produced by simulated pyrolysis of a PMHS/DVB polymer is shown in Figure 10.

4. CONCLUSIONS

We developed new ReaxFF potential parameters for interactions among elements Si, C, O, and H through optimization and learning algorithms. The force field shows excellent agreement with DFT calculations for energy differences for a vast variety of compositions and configurations. Moreover, local minima on the potential energy surfaces of both methods agree with each other. The force field demonstrates its predictive capability in simulations of thermal treatment of polysiloxanes. Modeling the polymer-to-ceramic conversion[14] of a cross-linked PHMS/DVB[65] polymer, we find remarkable

DOI: 10.1021/acs.jpcc.9b03810
J. Phys. Chem. C 2019, 123, 16804−16812

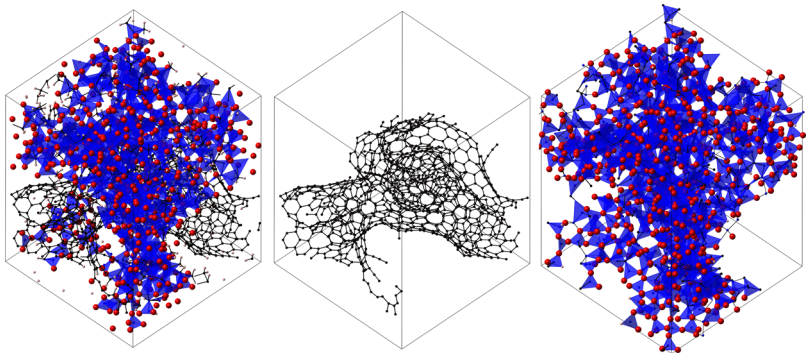

Figure 10. Structure of a-SiCO obtained by simulated annealing of the PMHS/DVB polymer precursor: the whole structure (left), free carbon phase (center), and a-SiCO phase (right).

Table 4. Annealing of the PMHS/DVB Polymer Precursor with the PMHS/DVB Mass Ratio of 2:1—Computations vs Experiment[a]

			composition [mass %]				
property	ρ [g/cm^3]	mass loss [%]	Si	C	O	H	C_{free}
simulation	2.02	22.6	39.2	38.1	21.8	0.9	32.8
experiment[4,51,73]	1.95	23	38.1	40.3	21.3	0.3	32

[a]"C_{free}" represents mass % of continuous C structure, not attached to Si.

agreement of composition, mass loss, and density of ceramic between experimental data[4,51,73,74] and simulation.

The force field enables simulations of fundamental chemical reactions in synthesis and processing of new materials. This encompasses new SiCO ceramic materials, synthesized either by a polymer-to-ceramic route or via the sol–gel process. Preliminary results show successful simulations of condensation reactions for trimethylethoxysilane into a gel-type system. Further applications are reactions occurring during the deposition of low-κ dielectric SiCO/H materials, as well as thermal treatment of these materials (post or concurrent synthesis) in reactive atmospheres such as H_2O, CO_2, or H_2. Future direction involves thermodynamic and kinetic stability of dielectric films,[75] thermal conductivity,[76] and the effects of radiation damage[8,77] or ion implantation.[75] Obviously, force field development is an ongoing process with room for improvement and progress. Adding additional elements, especially N and B, will broaden the scope of applications. With concurrent computer facilities, it becomes possible to perform simulations of several nanoseconds on the length scale of several nanometers with fidelity comparable to quantum chemical calculations.

AUTHOR INFORMATION

Corresponding Author

*E-mail: pkroll@uta.edu.

ORCID

Ilia Ponomarev: 0000-0002-3321-6671

Adri C. T. van Duin: 0000-0002-3478-4945

Peter Kroll: 0000-0003-4782-2805

Notes

The authors declare no competing financial interest.

ACKNOWLEDGMENTS

This work was supported by NSF, award CMMI-1634448. ACTvD acknowledges funding from DoE grant DE-EE008195. Computational work was made possible through generous grants by the Texas Advance Computing Center in Austin, TACC, Texas and UTA HPC facilities.

REFERENCES

(1) Sorarù, G. D.; Modena, S.; Guadagnino, E.; Colombo, P.; Egan, J.; Pantano, C. Chemical Durability of Silicon Oxycarbide Glasses. *J. Am. Ceram. Soc.* **2002**, *85*, 1529–1536.

(2) Rouxel, T.; Massouras, G.; Sorarù, G.-D. High Temperature Behavior of a Gel-Derived SiOC Glass: Elasticity and Viscosity. *J. Sol-Gel Sci. Technol.* **1999**, *14*, 87–94.

(3) Walter, S.; Soraru, G. D.; Bréquel, H.; Enzo, S. Microstructural and Mechanical Characterization of Sol Gel-Derived Si-O-C Glasses. *J. Eur. Ceram. Soc.* **2002**, *22*, 2389–2400.

(4) Soraru, G. D.; Kundanati, L.; Santhosh, B.; Pugno, N. Influence of Free Carbon on the Young's Modulus and Hardness of Polymer–Derived Silicon Oxycarbide Glasses. *J. Am. Ceram. Soc.* **2019**, *102*, 907–913.

(5) Lee, L.-L.; Tsai, D.-S. A Hydrogen-Permselective Silicon Oxycarbide Membrane Derived from Polydimethylsilane. *J. Am. Ceram. Soc.* **2004**, *82*, 2796–2800.

(6) Juttke, Y.; Richter, H.; Voigt, I.; Prasad, R. M.; Bazarjani, M. S.; Gurlo, A.; Riedel, R. Polymer Derived Ceramic Membranes for Gas Separation. *ICheaP-11: 11th International Conference on Chemical and Process Engineering, Pts 1-4*, 2013; Vol. *32*, pp 1891–1896.

(7) Chiang, C.-C.; Ko, I.-H.; Chen, M.-C.; Wu, Z.-C.; Lu, Y.-C.; Jang, S.-M.; Liang, M.-S. Leakage and Breakdown Mechanisms of Cu Comb Capacitors with Bilayer-Structured α-SiCN/α-SiC Cu-Cap Barriers. *J. Electrochem. Soc.* **2004**, *151*, G612.

(8) Ding, H.; Demkowicz, M. J. Hydrogen Enhances the Radiation Resistance of Amorphous Silicon Oxycarbides. *Acta Mater.* **2017**, *136*, 415–424.

(9) Nastasi, M.; Su, Q.; Price, L.; Colón Santana, J. A.; Chen, T.; Balerio, R.; Shao, L. Superior Radiation Tolerant Materials: Amorphous Silicon Oxycarbide. *J. Nucl. Mater.* **2015**, *461*, 200–205.

(10) Tamayo, A.; Ruiz-Caro, R.; Mazo, A.; Veiga-Ochoa, M. D.; Rubio, J. Chemical Oxidation of Silicon Oxycarbide Ceramics for Advanced Drug Delivery Systems. *J. Mater. Sci.* **2016**, *51*, 1382–1391.

(11) Suyal, N.; Krajewski, T.; Mennig, M. Microstructural and Dielectric Characterization of Sol-Gel Derived Silicon Oxycarbide Glass Sheets. *J. Sol-Gel Sci. Technol.* **1999**, *14*, 113–123.

DOI: 10.1021/acs.jpcc.9b03810
J. Phys. Chem. C 2019, 123, 16804–16812

(12) David, L.; Bhandavat, R.; Barrera, U.; Singh, G. Silicon Oxycarbide Glass-Graphene Composite Paper Electrode for Long-Cycle Lithium-Ion Batteries. *Nat. Commun.* **2016**, *7*, 10998.
(13) Pantano, C. G.; Singh, A. K.; Zhang, H. Silicon Oxycarbide Glasses. *J. Sol-Gel Sci. Technol.* **1999**, *14*, 7−25.
(14) Colombo, P.; Mera, G.; Riedel, R.; Soraru, G. D. Polymer-Derived Ceramics: 40 Years of Research and Innovation in Advanced Ceramics. *J. Am. Ceram. Soc.* **2010**, *93*, 1805−1837.
(15) Gallis, S.; Nikas, V.; Huang, M.; Eisenbraun, E.; Kaloyeros, A. E. Comparative Study of the Effects of Thermal Treatment on the Optical Properties of Hydrogenated Amorphous Silicon-Oxycarbide. *J. Appl. Phys.* **2007**, *102*, 024302.
(16) Rouessac, V.; Favennec, L.; Rémiat, B.; Jousseaume, V.; Passemard, G.; Durand, J. Precursor Chemistry for ULK CVD. *Microelectron. Eng.* **2005**, *82*, 333−340.
(17) Ryan, J. V.; Pantano, C. G. Synthesis and Characterization of Inorganic Silicon Oxycarbide Glass Thin Films by Reactive RF-Magnetron Sputtering. *J. Vac. Sci. Technol., A* **2007**, *25*, 153−159.
(18) Bréquel, H.; Parmentier, J.; Walter, S.; Badheka, R.; Trimmel, G.; Masse, S.; Latournerie, J.; Dempsey, P.; Turquat, C.; Desmartin-Chomel, A.; et al. Systematic Structural Characterization of the High-Temperature Behavior of Nearly Stoichiometric Silicon Oxycarbide Glasses. *Chem. Mater.* **2004**, *16*, 2585−2598.
(19) Das, G.; Mariotto, G.; Quaranta, A. Microstructural Evolution of Thermally Treated Low-Dielectric Constant SiOC:H Films Prepared by PECVD. *J. Electrochem. Soc.* **2006**, *153*, F46−F51.
(20) Bois, L.; Maquet, J.; Babonneau, F.; Mutin, H.; Bahloul, D. Structural Characterization of Sol-Gel Derived Oxycarbide Glasses. 1. Study of the Pyrolysis Process. *Chem. Mater.* **1994**, *6*, 796−802.
(21) Nimmo, J. P.; Kroll, P. First-Principles Calculations and Analysis of 29Si Nuclear Magnetic Resonance Chemical Shifts in Silicon Oxycarbide Ceramics. *J. Phys. Chem. C* **2014**, *118*, 29952−29961.
(22) Mera, G.; Navrotsky, A.; Sen, S.; Kleebe, H.-J.; Riedel, R. Polymer-Derived SiCN and SiOC Ceramics - Structure and Energetics at the Nanoscale. *J. Mater. Chem. A* **2013**, *1*, 3826−3836.
(23) Mera, G.; Gallei, M.; Bernard, S.; Ionescu, E. Ceramic Nanocomposites from Tailor-Made Preceramic Polymers. *Nanomaterials* **2015**, *5*, 468−540.
(24) Stabler, C.; Ionescu, E.; Graczyk-Zajac, M.; Gonzalo-Juan, I.; Riedel, R. Silicon oxycarbide glasses and glass-ceramics: "All-Rounder" materials for advanced structural and functional applications. *J. Am. Ceram. Soc.* **2018**, *101*, 4817−4856.
(25) Kroll, P. Modelling and Simulation of Amorphous Silicon Oxycarbide. *J. Mater. Chem.* **2003**, *13*, 1657−1668.
(26) Kroll, P. Searching Insight into the Atomistic Structure of SiCO Ceramics. *J. Mater. Chem.* **2010**, *20*, 10528−10534.
(27) Marshall, D.; Cox, B.; Kroll, P.; Hilmas, G.; Fahrenholtz, W.; Raj, R.; Ritchie, R.; Yang, Q.; Zok, F. *National Hypersonic Science Center for Materials and Structures*, Final Report, 2014.
(28) van Duin, A. C. T.; Dasgupta, S.; Lorant, F.; Goddard, W. A. ReaxFF: A Reactive Force Field for Hydrocarbons. *J. Phys. Chem. A* **2001**, *105*, 9396−9409.
(29) Soria, F. A.; Zhang, W.; van Duin, A. C. T.; Patrito, E. M. Thermal Stability of Organic Monolayers Grafted to Si(111): Insights from ReaxFF Reactive Molecular Dynamics Simulations. *ACS Appl. Mater. Interfaces* **2017**, *9*, 30969−30981.
(30) Soria, F. A.; Zhang, W.; Paredes-Olivera, P. A.; van Duin, A. C. T.; Patrito, E. M. Si/C/H ReaxFF Reactive Potential for Silicon Surfaces Grafted with Organic Molecules. *J. Phys. Chem. C* **2018**, *122*, 23515−23527.
(31) Newsome, D. A.; Sengupta, D.; Foroutan, H.; Russo, M. F.; van Duin, A. C. T. Oxidation of Silicon Carbide by O2 and H2O: A ReaxFF Reactive Molecular Dynamics Study, Part I. *J. Phys. Chem. C* **2012**, *116*, 16111−16121.
(32) Ding, H. P.; Demkowicz, M. J. Hydrogen Reverses the Clustering Tendency of Carbon in Amorphous Silicon Oxycarbide. *Sci. Rep.* **2015**, *5*, 13051.
(33) Gao, H.; Wang, H.; Zhao, Z.; Niu, M.; Su, L.; Wei, Y. Reactive Dynamics Simulation Study on the Pyrolysis of Polymer Precursors to Generate Amorphous Silicon Oxycarbide Structures. *J. Phys. Chem. C* **2018**, *122*, 5767−5773.
(34) Srinivasan, S. G.; van Duin, A. C. T.; Ganesh, P. Development of a ReaxFF Potential for Carbon Condensed Phases and Its Application to the Thermal Fragmentation of a Large Fullerene. *J. Phys. Chem. A* **2015**, *119*, 571−580.
(35) Bodifort, N. Crystalline SiCO: Implication on Structure and Thermochemistry of Ternary Silicon Oxycarbide Ceramics. M.S. Thesis, The University of Texas at Arlington, 2013.
(36) Wooten, F.; Winer, K.; Weaire, D. Computer Generation of Structural Models of Amorphous Si and Ge. *Phys. Rev. Lett.* **1985**, *54*, 1392−1395.
(37) Kroll, P. Structure and Reactivity of Amorphous Silicon Nitride Investigated with Density-Functional Methods. *J. Non-Cryst. Solids* **2001**, *293−295*, 238−243.
(38) Hohenberg, P.; Kohn, W. Inhomogeneous Electron Gas. *Phys. Rev. B: Condens. Matter Mater. Phys.* **1964**, *136*, B864.
(39) Kresse, G.; Hafner, J. Ab initiomolecular-dynamics simulation of the liquid-metal-amorphous-semiconductor transition in germanium. *Phys. Rev. B: Condens. Matter Mater. Phys.* **1994**, *49*, 14251−14269.
(40) Kresse, G.; Furthmüller, J. Efficiency of Ab-Initio Total Energy Calculations for Metals and Semiconductors Using a Plane-Wave Basis Set. *Comput. Mater. Sci.* **1996**, *6*, 15−50.
(41) Blöchl, P. E. Projector Augmented-Wave Method. *Phys. Rev. B: Condens. Matter Mater. Phys.* **1994**, *50*, 17953−17979.
(42) Kresse, G.; Joubert, D. From Ultrasoft Pseudopotentials to the Projector Augmented-Wave Method. *Phys. Rev. B: Condens. Matter Mater. Phys.* **1999**, *59*, 1758−1775.
(43) Perdew, J. P.; Burke, K.; Ernzerhof, M. Generalized Gradient Approximation Made Simple. *Phys. Rev. Lett.* **1996**, *77*, 3865−3868.
(44) Perdew, J. P.; Burke, K.; Ernzerhof, M. Generalized Gradient Approximation Made Simple [Phys. Rev. Lett. 77, 3865 (1996)]. *Phys. Rev. Lett.* **1997**, *78*, 1396.
(45) Grimme, S. Semiempirical GGA-Type Density Functional Constructed with a Long-Range Dispersion Correction. *J. Comput. Chem.* **2006**, *27*, 1787−1799.
(46) Plimpton, S. Fast Parallel Algorithms for Short-Range Molecular Dynamics. *J. Comput. Phys.* **1995**, *117*, 1−19.
(47) Aktulga, H. M.; Fogarty, J. C.; Pandit, S. A.; Grama, A. Y. Parallel Reactive Molecular Dynamics: Numerical Methods and Algorithmic Techniques. *Parallel Comput.* **2012**, *38*, 245−259.
(48) Bussi, G.; Donadio, D.; Parrinello, M. Canonical Sampling through Velocity Rescaling. *J. Chem. Phys.* **2007**, *126*, 014101.
(49) Hornetz, B.; Michel, H.-J.; Halbritter, J. ARXPS studies of SiO2-SiC interfaces and oxidation of 6H SiC single crystal Si-(001) and C-(001) surfaces. *J. Mater. Res.* **1994**, *9*, 3088−3094.
(50) Önneby, C.; Pantano, C. G. Silicon oxycarbide formation on SiC surfaces and at the SiC/SiO2 interface. *J. Vac. Sci. Technol., A* **1997**, *15*, 1597−1602.
(51) Dibandjo, P.; Diré, S.; Babonneau, F.; Soraru, G. D. Influence of the Polymer Architecture on the High Temperature Behavior of SiCO Glasses: A Comparison between Linear- and Cyclic-Derived Precursors. *J. Non-Cryst. Solids* **2010**, *356*, 132−140.
(52) Takamoto, S.; Yamasaki, T.; Ohno, T.; Kaneta, C.; Hatano, A.; Izumi, S. Elucidation of the Atomic-Scale Mechanism of the Anisotropic Oxidation Rate of 4H-SiC between the (0001) Si-Face and (000(1)over-Bar) C-Face by Using a New Si-O-C Interatomic Potential. *J. Appl. Phys.* **2018**, *123*, 185303.
(53) Rouxel, T.; Soraru, G.-D.; Vicens, J. Creep Viscosity and Stress Relaxation of Gel-Derived Silicon Oxycarbide Glasses. *J. Am. Ceram. Soc.* **2001**, *84*, 1052−1058.
(54) Shiina, K.; Kumada, M. Notes - Thermal Rearrangement of Hexamethyldisilane to Trimethyl(dimethylsilylmethyl)silane. *J. Org. Chem.* **1958**, *23*, 139.

DOI: 10.1021/acs.jpcc.9b03810
J. Phys. Chem. C 2019, 123, 16804−16812

(55) Radovanovic, E.; Gozzi, M. F.; Gonçalves, M. C.; Yoshida, I. V. P. Silicon Oxycarbide Glasses from Silicone Networks. *J. Non-Cryst. Solids* **1999**, *248*, 37−48.
(56) Yu, Y.; Wang, B.; Wang, M.; Sant, G.; Bauchy, M. Revisiting Silica with Reaxff: Towards Improved Predictions of Glass Structure and Properties Via Reactive Molecular Dynamics. *J. Non-Cryst. Solids* **2016**, *443*, 148−154.
(57) Pitman, M. C.; van Duin, A. C. T. Dynamics of Confined Reactive Water in Smectite Clay-Zeolite Composites. *J. Am. Chem. Soc.* **2012**, *134*, 3042−3053.
(58) Mazurin, O. V.; Streitsina, M. V.; Shvaiko-Shvaikovskaya, T. P. *Handbook of Glass Science, Volume 15A: Silica Glass and Binary Silicate Glasses*; Elsevier Science Publishers B.V., 1983.
(59) Tersoff, J. Empirical Interatomic Potential for Silicon with Improved Elastic Properties. *Phys. Rev. B: Condens. Matter Mater. Phys.* **1988**, *38*, 9902−9905.
(60) Tersoff, J. Empirical Interatomic Potential for Carbon, with Applications to Amorphous Carbon. *Phys. Rev. Lett.* **1988**, *61*, 2879−2882.
(61) Kroll, P. Computersimulationen und Röntgennahkantenabsorptionsspektroskopie von Siliciumnitrid und Siliciumcarbidnitrid Keramiken. Ph.D. Dissertation, TU Darmstadt, 1996.
(62) Munetoh, S.; Motooka, T.; Moriguchi, K.; Shintani, A. Interatomic Potential for Si-O Systems Using Tersoff Parameterization. *Comput. Mater. Sci.* **2007**, *39*, 334−339.
(63) Chatgilialoglu, C. Structural and Chemical Properties of Silyl Radicals. *Chem. Rev.* **1995**, *95*, 1229−1251.
(64) Liao, N.; Xue, W.; Zhou, H.; Zhang, M. Molecular Dynamics Investigation of Structure and High-Temperature Mechanical Properties of SiBCO Ceramics. *J. Alloys Compd.* **2014**, *610*, 45−49.
(65) Blum, Y. D.; MacQueen, D. B.; Kleebe, H.-J. Synthesis and Characterization of Carbon-Enriched Silicon Oxycarbides. *J. Eur. Ceram. Soc.* **2005**, *25*, 143−149.
(66) Lu, K. Porous and High Surface Area Silicon Oxycarbide-Based Materials-a Review. *Mater. Sci. Eng. R Rep.* **2015**, *97*, 23−49.
(67) Kleebe, H.-J.; Blum, Y. D. SiOC Ceramic with High Excess Free Carbon. *J. Eur. Ceram. Soc.* **2008**, *28*, 1037−1042.
(68) Sasikumar, P. V. W.; Zera, E.; Graczyk-Zajac, M.; Riedel, R.; Soraru, G. D. Structural Design of Polymer-Derived SiOC Ceramic Aerogels for High-Rate Li Ion Storage Applications. *J. Am. Ceram. Soc.* **2016**, *99*, 2977−2983.
(69) Graczyk-Zajac, M.; Vrankovic, D.; Waleska, P.; Hess, C.; Sasikumar, P. V.; Lauterbach, S.; Kleebe, H.-J.; Sorarù, G. D. The Li-Storage Capacity of SiOC Glasses with and without Mixed Silicon Oxycarbide Bonds. *J. Mater. Chem. A* **2018**, *6*, 93−103.
(70) Liao, N.; Zhou, H.; Zheng, B.; Xue, W. Silicon Oxycarbide-Derived Carbon as Potential NO2 Gas Sensor: A First Principles' Study. *IEEE Electron. Device Lett.* **2018**, *39*, 1760−1763.
(71) Du, T.; Li, H.; Sant, G.; Bauchy, M. New Insights into the Sol-Gel Condensation of Silica by Reactive Molecular Dynamics Simulations. *J. Chem. Phys.* **2018**, *148*, 234504.
(72) Sorarù, G. D.; Pederiva, L.; Latournerie, J.; Raj, R. Pyrolysis Kinetics for the Conversion of a Polymer into an Amorphous Silicon Oxycarbide Ceramic. *J. Am. Ceram. Soc.* **2002**, *85*, 2181−2187.
(73) Pradeep, V. S. Study of Silicon Oxycarbide (SiOC) as Anode Materials for Li-Ion Batteries. Ph.D. Dissertation, University of Trento, 2013.
(74) Hourlier, D.; Venkatachalam, S.; Ammar, M.-R.; Blum, Y. Pyrolytic Conversion of Organopolysiloxanes. *J. Anal. Appl. Pyrolysis* **2017**, *123*, 296−306.
(75) Chen, J.; Calvin, J.; Asplund, M.; King, S. W.; Woodfield, B. F.; Navrotsky, A. Heat Capacities, Entropies, and Gibbs Free Energies of Formation of Low-K Amorphous Si(O)CH Dielectric Films and Implications for Stability During Processing. *J. Chem. Thermodyn.* **2019**, *128*, 320−335.
(76) Harikrishna, H.; Lanford, W. A.; King, S. W.; Huxtable, S. T. Thermal Conductivity of Plasma Deposited Amorphous Hydrogenated Boron and Carbon Rich Thin Films. *J. Nucl. Mater.* **2019**, *514*, 154−160.
(77) Su, Q.; Wang, T.; Gigax, J.; Shao, L.; Lanford, W. A.; Nastasi, M.; Li, L.; Bhattarai, G.; Paquette, M. M.; King, S. W. Influence of Topological Constraints on Ion Damage Resistance of Amorphous Hydrogenated Silicon Carbide. *Acta Mater.* **2019**, *165*, 587−602.

DOI: 10.1021/acs.jpcc.9b03810
J. Phys. Chem. C 2019, 123, 16804−16812